EUROPEAN ORGANIZATION FOR NUCLEAR RESEARCH

CERN/PSCC/84-67
PSCC/P 80
21 December 1984

PROPOSAL TO THE PSCC

SPECTROSCOPY AT LEAR USING AN INTERNAL HYDROGEN JET TARGET

Annecy (LAPP)[1]-CERN[2]-Genoa[3]-Oslo[4] Collaboration

G. Bassompierre[1], L. Bugge[4], A. Buzzo[3], M. Dameri[3], T. Fearnley[4], S. Ferroni[3], E. Khan[2], K. Kirsebom[4], A. Kylling[4], A. Lundby[2], M. Macri[3], M. Marinelli[3], L. Mattera[3], B. Mouellic[2], D. Olsen[4], B. Osculati[3], M.G. Pia[3], A. Santroni[3], S. Stapnes[4], B. Stugu[4], F. Tommasini[3] and U. Valbusa[3]

ABSTRACT

In our Letter of Intent PSCC/84-22/I 67 we proposed to transfer the hydrogen jet target from the ISR to LEAR. While at the ISR we looked at charmonium states formed in $p\bar{p}$ annihilations, we would at LEAR study multi-gluon (gluonium) or multi-quark states or hybrids in formation experiments. The smaller diameter of the LEAR ring could give us luminosities about 10 times higher than at the ISR. The cooling time of the antiprotons should also be much shorter, and the final mass resolution $\leq$ 100 keV.

We would look at two-body final states such as $\phi\phi$, and we propose to scan the energy range from the $\phi\phi$ threshold ($\bar{p}$ momentum 0.87 GeV/c) across the ξ (2.22 GeV) resonance and the $g_T(2.12)$ and $g_T(2.36)$ resonances.

GENEVA
1984

1. PHYSICS MOTIVATION

In the centre-of-mass energy range available at LEAR, the existence of states with exotic composition (multi-quark states, glueballs or hybrids) [1] has been predicted by models stemming from the general axioms of Quantum Chromodynamics. These predictions have not so far been confirmed by experiment, even if indications exist for a rich structure in this energy range. Recent experimental evidence has been found for a narrow state at 2.22 GeV in the radiative decay of the J/ψ [2]. Many speculations have been presented as to the nature of this state: apart from its possible interpretation as an excited $q\bar{q}$ system the possibility that it is a tensor glueball [3], a technipion [4], a multiquark state [5], or a Higgs [6] has been discussed. A precise knowledge of the state parameters (total width, coupling, etc.) will be essential in order to resolve the issue. The same remarks apply to the $\phi\phi$ resonances seen in a Brookhaven experiment in the Okubo-Zweig-Iizuka (OZI) forbidden reaction $\pi^- p \rightarrow \phi\phi n$ at 22 GeV/c [7].

Many models also suggest the existence of hadrons consisting of 'molecules' of colour substructures (baryonium), and several LEAR experiments are examining this question.

In the proposed formation experiment, the mass and the width of the resonance will be determined directly by the machine parameters (momentum and momentum spread of the coasting beam), and a precision of $\leq$ 100 keV can be obtained. The final-state detector should only provide a clean signature of the resonance decay. The choice of the decay channel to be selected is important since it can provide information on the quantum numbers of the resonance under study and on its constituent composition. We propose to detect preferentially quasi-two-body final states with $s\bar{s}$ content ($K^0_S K^0_S$, $\phi\phi$). This will, on the one hand, enhance the signal/background ratio, and, on the other hand, it is expected that the exotic states decay abundantly into strange particles. Moreover, it is well known that a Higgs particle couples preferentially to high-mass fermions, again favouring strange particles in the final states. The following channel is particularly interesting:

$$p\bar{p} \rightarrow \phi\phi \rightarrow K^+ + K^- + K^+ + K^- . \qquad (1)$$

A strong physics motivation for studying this channel is that ϕ is practically pure $s\bar{s}$, which implies that the reaction goes predominantly through a gluonic intermediate state. The non-resonant cross-section for this reaction is low, being OZI suppressed, while the signature is constrained by the low Q value of the decay. The threshold for this channel is at $\sqrt{s}$ = 2040 MeV, that is to say for a momentum of the coasting beam of 0.87 GeV/c.

The resonance at 2.22 GeV (ξ) provides a good example of the possibilities of this experiment. Two characteristics make this state very interesting: a) its narrow width ($\Gamma \leq$ 30 MeV compatible with the resolution of the MARK III detector), b) the fact that it has an anomalously high branching ratio into KK. Combining the information from the inclusive spectrum (Crystal Ball) and from the $J/\psi \rightarrow \gamma\xi \rightarrow \gamma K^+K^-$ rate (MARK III), we estimate the branching ratio to KK to be of the order of 20-30%. The fact that it is observed to decay to $K^0_S K^0_S$ establishes its quantum numbers to be $J^{PC} = 0^{++}, 2^{++}...$; it should, therefore, also decay into $\phi\phi$. In the MARK III experiment the detection of the $\phi\phi$ final state was difficult. Finding the $\xi(2.22)$ in this final state and performing an accurate scan around the formation energy in $p\bar{p}$ annihilation would allow the measurement of the strength of the ξ coupling to the $p\bar{p}$ channel and the determination with great accuracy of its width. Both these pieces of information are essential in order to establish the nature of the state.

2. H_2 JET TARGET IN LEAR

The target we propose to install in LEAR was already used in experiment R704 at the ISR. It has been described in detail [8, 9]. The flux of H_2 clusters is generated from the expansion of H_2 at low temperature and high pressure through a special injector of very small (30 μm) diameter. The flux of H_2 traversing the LEAR vacuum chamber is absorbed in a sink system. The flux of H_2 dispersed in the machine vacuum pipe from the production and sink is minimized by interposing additional pumping systems.

The general layout is shown in Figs. 1a and b. The target dimensions are matched to the $\bar{p}$ beam by a system of collimators. The intensity of the gas source is such that the target thickness traversed by the $\bar{p}$ beam has a maximum value of 1.5×10^{14} atoms per square centimetre = $2.5 \times 10^{-10}\,g \cdot cm^{-2}$.

The only direct effect of the jet on the ring pressure comes from the H_2 back-streaming from the sink and the H_2 flowing from the production stage but not trapped in the sink system. The experience at the ISR is that this amount of gas can be reduced to less than 2% of the gas in the jet. The lifetime and the momentum resolution of the $\bar{p}$ beam depend mainly on the jet density and the actual performance of the cooling system.

We foresee three running modes with the target:

i) Parasitic to antiproton slow extraction for external beam use.

ii) Dedicated running periods.

iii) A very attractive possibility is, as mentioned in our Letter of Intent [10], to run the target during the periods of sharing with the SPS $p\bar{p}$ Collider. During these periods a low-intensity (5×10^9 $\bar{p}$) pulse (which is $\simeq$ 5% of the AA accumulation per day) could be transferred to LEAR, and the target thickness should be chosen in such a way that this $\bar{p}$ pulse would be used in a one-day cycle. This density is $= 7 \times 10^{13}$ atoms per square centimetre = $1.2 \times 10^{-10}\,g \cdot cm^{-2}$ of H_2. The corresponding initial luminosity is $2.5 \times 10^{30}\,cm^{-2}\,s^{-1}$. If the performance of the stochastic cooling system is as anticipated we would integrate a luminosity $\simeq 50\,nb^{-1}$ per day and per 5×10^9 antiprotons injected.

The main requirement on the LEAR operation is then that the central value of the momentum distribution of the $\bar{p}$ beam can be displaced in very small steps or even continuously by the stochastic cooling system itself. This would allow the reconstruction of the excitation functions of the resonances.

3. EXPERIMENTAL SET-UP

3.1 Introduction

The first reaction we would like to study is

$$p\bar{p} \rightarrow \phi\phi \rightarrow K^+ + K^- + K^+ + K^-$$

with $\bar{p}$ momenta from 870 MeV/c (threshold) to the maximum available in LEAR.

3.2 Detection

The apparatus (Figs. 2a and b) consists of a two-arm non-magnetic spectrometer surrounded by scintillation counters to veto multiparticle final states (> 4). Each arm (Fig. 2b) is composed of multiwire proportional chambers (MWPCs) CH1 and CH2 for track reconstruction and dE/dx measurements, a sandwich of sheets of Pb and scintillating optical fibres for the measurement of the range, and scintillation counter hodoscopes for the trigger definition. The π, K, p discrimination is based on the simultaneous measurements of dE/dx and of the range

of the final-state particles. This method can be applied since the momenta of Ks from $\phi\phi \rightarrow K^+K^-K^+K^-$ decays are below 750 MeV/c. Their spectrum is shown in Fig. 3. As shown in Fig. 4 (a to f) it is possible to define a dE/dx range correlation by which the kaons are identified.

The following requirements should be taken into account in the definition of the correlations:

a) high efficiency for K identification,

b) high rejection power of π, p,

c) a very compact apparatus imposed by the short K-decay length.

A Monte Carlo calculation performed in order to evaluate the rejection power of this method against background reactions will be discussed in subsection 4.2.

The analogue MWPC system in each arm consists of two chambers of five active planes each giving a total of 10 dE/dx samplings for each detected final-state particle. Using the 50% truncated mean method we obtain, from a Monte Carlo simulation, the results shown in Fig. 5.

For comparison we have applied the same algorithm to experimental data on minimum ionizing particles detected in experiment R704 with a system of four analogue MWPCs. It reduces the uncertainty in the energy-loss measurement due to the Landau fluctuations (Fig. 6a and b). The structure of each gap is shown in Fig. 7. We use the same construction technique as for the analogue MWPC used for experiment R704 at the ISR [9]. Figure 8 shows the reconstructed peaks obtained from the two lines of the ^{55}Fe.

The range detector is an important part of the apparatus. The measurement of the range of the $K^{\pm}$ ($\pi^{\pm}$, p, $\bar{p}$) is not easy because in addition to the primary particles we have decay particles and interaction products. We would therefore have a fine transversal and longitudinal segmentation of the detector, that is to say many layers of detection planes built from hodoscopes of scintillating optical fibres in different orientations interleaved with Pb layers. Full information (pattern of hit hodoscopes and pulse height of each counter) will be used to obtain a complete understanding of the event. The sampling (number of planes and Pb thickness) is based on Monte Carlo calculations, the criteria being that the energy loss–range correlation should be fully exploited. To take into account the complexity of the event we have added more planes to those just needed for the correlation. In fact additional identification can be obtained by measuring the pulse height in the fibre planes before the particle stops. The main parameters for one range detector are summarized in Table 1.

A special way of grouping the fibres onto the photomultipliers (PMs) makes it possible to obtain a good spatial resolution combined with a reasonable number of readout channels (= No. of PMs). The principle is illustrated in Fig. 9. With eight PMs one obtains a resolution corresponding to the width of a single fibre, while the number of fibres per layer is twice as many. With this technique multihits and layer inefficiencies may lead to ambiguities in the pattern recognition. This problem has been circumvented by adding at least one fibre layer to the basic configuration of each plane.

The fibres will be approximately 1.2 m in length. The bundles of fibres (containing from 100 to 300 fibres) are viewed by EMI 9826B phototubes (bialkaline, 13 mm cathode diameter, 12 stage and linear focus). It should be noted that all channels will be read analogically.

We expect to observe on the average 5–6 photoelectrons [11] from the crossing of one layer (= 1 mm) by a minimum ionizing particle at a distance of 1 m from the PM. With at least three layers per plane (see Table 1) the signal should be well above the noise level of the PMs. As regards efficiency considerations we wish to point out that the filling factor will be considerably higher than that which would result from calculations on a structure such as the one presented in the cross-section of Fig. 9. The dead space may be greatly reduced by heating this structure in an appropriate mould: when the fibres expand they fill up the dead space and will not shrink when

returned to room temperature. This has been tried with success at CERN and has been found not to alter the attenuation properties of the fibres [12]. Heated fibre layers or planes naturally would exhibit higher efficiencies than the corresponding configurations unheated.

The fibres are sensitive to ionization all the way up to the PMs. This naturally is an inconvenience, in particular with our way of cabling the fibres. Hits outside the active part of the acceptance cannot easily be distinguished from those inside and hence may give rise to ambiguities in the pattern recognition. To meet this problem care will be taken so that the fibres' connections may easily be covered by veto counters. Also we want to investigate a technique [12] of soldering non-scintillating fibres onto the scintillating ones. This would very efficiently eliminate the problem.

3.3 Trigger

The trigger is based on the quasi two-body kinematics of reaction (1). Coincidence matrices between the scintillation counter hodoscopes which use the correlation pattern of the ϕ decay product will allow a powerful rejection against background. However, in order to impose the kinematical correlation and the multiplicity condition (two particles in each arm) only on tracks coming from the interaction region, we have to perform some filtering to reject backward particles coming from the range detector and due to decay or interaction products. This filtering could easily be done by setting alignment coincidence matrices. The system of scintillation counters surrounding the two detection arms will veto multiparticle ($n > 4$) final states.

The use of a microprocessor which can perform a refined geometrical correlation is envisaged at the last level of the trigger, before the data acquisition to the on-line computer.

3.4 Monitor

The monitoring and calibration of the luminosity can be obtained from elastic scattering measurements. We propose (as was already done in the ISR experiment R704 [9]) to detect the elastic protons recoiling at large angles and to measure their kinetic energy by means of solid-state detectors (Si surface-barrier detectors).

4. RATES AND BACKGROUND

4.1 Rates

The cross-section for annihilation through a resonance can be written as:

$$\sigma_d(E) = \pi\lambda\!\!\!^{-2}(2J + 1)\,\Gamma_p\Gamma_d / \{(2S_1 + 1)(2S_2 + 1)[(E - E_0)^2 + \Gamma^2/4]\}\,. \qquad (2)$$

where $\lambda\!\!\!^{-2} = (\hbar/p)^2$ with p being the c.m. momentum and $\hbar = 0.197$ fm·GeV/c; S_1, S_2, and J are the spin of the incident particle, target, and resonance, respectively; Γ_p, Γ_d, Γ are the partial decay widths into $\bar{p}p$, the final state, and the total width of the resonance, respectively.

The peak cross-section at the resonance is then:

$$\sigma_p\,(E = E_0) = 4\pi\,\hbar^2\,(2J + 1)\,\Gamma_p\Gamma_d/(E_0^2 - 4m_p^2)\,\Gamma^2\,. \qquad (3)$$

For a c.m. energy $\bar{E}$ corresponding to the central value of the $\bar{p}$ momenta distribution, the formation rate is given by:

$$R(\bar{E}) = \int_{\Delta M} L(E)\sigma(E)\,dE\,, \qquad (4)$$

L(E) being the luminosity density. The integration is over the c.m. energy spread ΔM:

$$\Delta M = \beta dp_{lab}/\sqrt{2}\,(1+\gamma)^{1/2} \tag{5}$$

and

$$\sigma(E) = \sigma_p\,\Gamma^2/[(E-E_0)^2 + \Gamma^2/4]\,. \tag{6}$$

4.2 Background

The identification of 4K final states is done by requiring an appropriate K-response, for each track, from the energy loss -range correlation described in Section 3.2.

The rejection power against various background reactions is calculated by a Monte Carlo method and summarized in Table 2.

Assuming a known momentum $\vec{p}$ of the $\bar{p}$ beam, the 4 measured directions allow a determination of the 4 particle momenta on the assumption of $\phi\phi \rightarrow$ 4K kinematics. Since we have 6 constraining equations for the 4 unknowns, the 2 superfluous equations can be used to filter away background. The rejection power for this kinematical filter with appropriate cuts is again given for various background channels in Table 2.

Since the energy loss-range correlation cut and the kinematical filter are largely uncorrelated, their combined rejection power is given by the product of the single rejection powers. This is indicated in columns 6 and 7 of Table 2.

With a momentum assignment to each track from the kinematics, additional rejection power comes from requiring a range-momentum correlation consistent with a K for each track. Column 8 of Table 2 indicates the level of background accepted by the coincidence of an energy loss-range correlation, kinematical filter, and range-momentum correlation.

Table 3 summarizes the event rate for detection with different hypotheses for the formation and decay rate. They are calculated according to expression (4).

REFERENCES

[1] C.E. DeTar and J.F. Donoghue, Bag models of hadrons, Ann. Rev. Nucl. Part. Sci. **33**, 235 (1983).

[2] MARK III Collaboration, K.F. Einsweiler et al., SLAC Pub. 3202 (1983).

[3] F. Close, Gluonic excitation in hadronic spectroscopy, Rutherford Laboratory report 83-090 (1983).

[4] H.E. Jaber, Can the $\xi(2.22)$ be a technipion? SLAC Pub. 3193 (1983).

[5] S. Pakvasa et al., Phys. Lett. **145B**, 135 (1984).

[6] H.E. Jaber and G.L. Kane, Some tests for whether a narrow neutral resonance can be a Higgs particle, SLAC Pub. 3209 (1983).

[7] A. Etkin et al., Phys. Rev. Lett. **49**, 1620 (1982).
S. Lindenbaum, Proc. Int. Europhysics Conf. on High Energy Physics, Brighton, 1983 (Rutherford Appleton Laboratory, Chilton, 1983), p. 351.

[8] M. Macri, A clustered H_2 beam, *in* Physics with Low Energy Cooled Antiprotons (Plenum, New York, 1983), p. 432.

[9] C. Baglin et al., Charmonium spectroscopy at the ISR using an antiproton beam and a H_2 gas jet target, EP preprint in preparation.

[10] C. Baglin et al., Letter of Intent, CERN/PSCC/84-22, PSCC/I 67 (1984).

[11] H. Burmeister et al., Nucl. Instrum. Method **225**, 530 (1984).

[12] D. Perrin and R. Famy, private communication.

Table 1

Range detector parameters

Plane No.	Pb thickness (cm)	Side [a] (cm)	Orientation [b]	Resolution [c] (cm) x	Resolution [c] (cm) y	No. of layers x	No. of layers y	No. of PMs [d]
1	1.5	61.5	x, y	1.0	1.0	3	2	27
2	1.5	64.0	x	0.5		3		12
3	2.5	66.5	y		0.5		4	16
4	2.5	70.0	x	0.5		4		17
5	2.5	72.5	y		0.5		4	17
6	2.5	75.0	x	0.5		4		17
7	2.5	77.5	y		0.5		4	17
8	2.5	81.6	x, y	0.85	0.85	4	3	26
				Total		35		149

a) The sensitive detector surface is square in shape seen from the $p\bar{p}$ vertex. The side of the square is approximately equal to the distance to the vertex.

b) x: vertical fibres, y: horizontal fibres.

c) Spatial resolution: 2 × resolution = minimum channel width.

d) Assuming 1 mm fibre diameter and a special way of cabling the fibres onto the PMs.

Table 2

Backgrounds

Reaction[a]	I = Geom. acceptance[b] (%)	A = (R,dE/dx) correlation[c] (%)	B = kin. fit (%)	C = Range momentum[d] (%)	A × B (%)	Total (A, B, C) (%)	Cross-section (μb)	Accepted background (nb)
$\bar{p}p \to 4K$ Non resonant	2.8 ± 0.1	90.5	27.6	15.9	25	9.2	4 ± 2	10.3 ± 5.2
$\bar{p}p \to 4\pi$	0.11 ± 0.01	< 0.1	< 0.1	< 0.1	$< 10^{-4}$	$< 10^{-4}$	2560^{+110}_{-150}	$< 10^{-2}$
$\bar{p}p \to 2K2\pi$	0.43 ± 0.01	< 0.1	< 0.1	< 0.1	$< 10^{-4}$	$< 10^{-4}$	350 ± 30	$< 10^{-2}$
$\bar{p}p \to \bar{p}p\pi\pi$	0.13 ± 0.01	9.8	14.8	0.7	0.94	$< 10^{-4}$	3 ± 2	$< 10^{-2}$
$\bar{p}p \to 5\pi^0$	0.18 ± 0.01	< 0.1	0.7	< 0.1	$< 10^{-4}$	$< 10^{-4}$	11200 ± 1000	$< 10^{-2}$
$\bar{p}p \to \pi\pi\phi$	0.79 ± 0.03	< 0.1	< 0.1	< 0.1	$< 10^{-4}$	$< 10^{-4}$	37 ± 25	$< 10^{-2}$

a) Uniformly generated in phase space, $p_{lab} = 1.398$ GeV/c.
b) Two particles inside each arm.
c) All limits at 95% confidence level.
d) Momentum value from kinematical fit to the hypothesis $\phi\phi \to 4K$.
e) For $\phi\phi \to 4K$ we obtain 99.1%.
f) $\bar{p}p \to \pi^+\pi^-\pi^+\pi^-\pi^0$, 2 charged π per arm, no requirement on π^0.

Table 3

ξ detection rate

Branching ratio of ξ to $\bar{p}p$	Branching ratio of ξ to $\phi\phi$	σ_{peak} (μb)	$\sigma_{accepted}$[a] (nb)	No. events[b] per hour	$\sigma_{back.\ acc.}$ (nb)	Signal background	Time to 7σ (h)
10^{-2}	10^{-2}	1.8	13.9	125	11	1.3	1
5×10^{-3}	10^{-2}	0.9	6.9	62	11	0.6	2
2×10^{-3}	10^{-2}	0.36	2.8	25	11	0.25	10

a) We assume $J_\xi = 2$; acceptance for $\xi \to \phi\phi$ is 3.3%.
BR ($\phi\phi \to K^+K^-K^+K^-$) = 24%.
b) Initial luminosity 2.5×10^{30} cm^{-2} s^{-1}, with 5×10^9 $\bar{p}$/per day, $\int_d L\,dt = 50$ nb^{-1}.

Figure captions

Fig. 1 : a) Top view of the H_2 target system.
b) Side view of the H_2 target system.

Fig. 2 : a) Schematic top view of the detection apparatus.
b) Side view of one detection arm.

Fig. 3 : Distribution of momentum of kaons from the decay of $\xi \rightarrow \phi\phi \rightarrow K^+K^-K^+K^-$ in the lab. system.

Fig. 4 : Distribution of energy loss of kaons in 1 cm · atm of argon for different intervals of kaon ranges.

Fig. 5 : a,b,c) Energy loss of kaons of fixed momentum (200, 400, 600 MeV/c) in 1 cm · atm of argon.
d,e,f) Same distributions as in (a,b,c), applying the algorithm described in the text.

Fig. 6 : a) Energy loss of a minimum ionizing proton measured in R704 MWPCs. Mean value of four gaps in 1 cm · atm of argon (Monte Carlo simulation).
b) Same distribution as in (a) from the truncated mean: two out of four gaps.

Fig. 7 : Schematic structure of one MWPC gap.

Fig. 8 : Energy loss of a ^{55}Fe source measured in the MWPC system of R704.

Fig. 9 : Range detector: method of assembly of fibres.

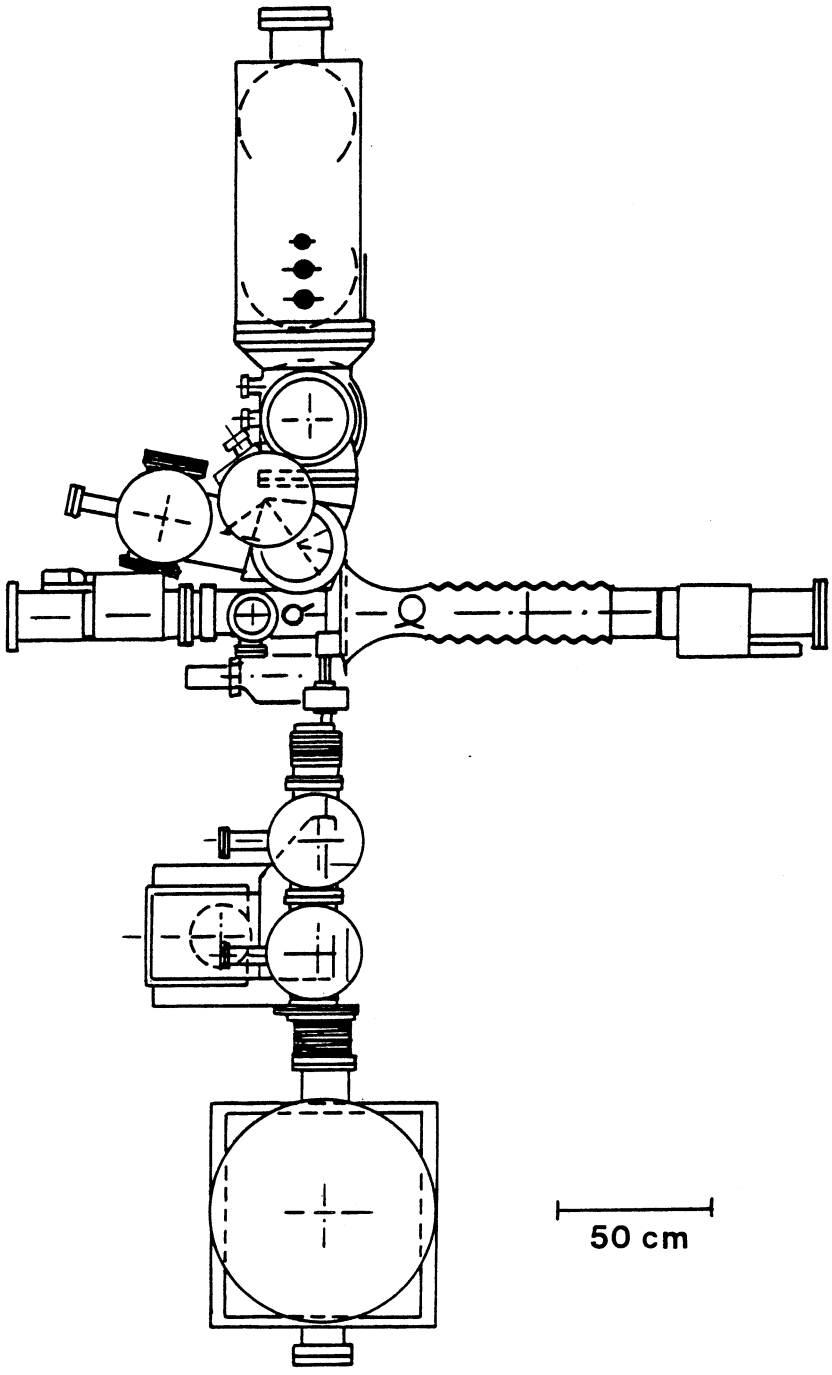

Fig. 1a

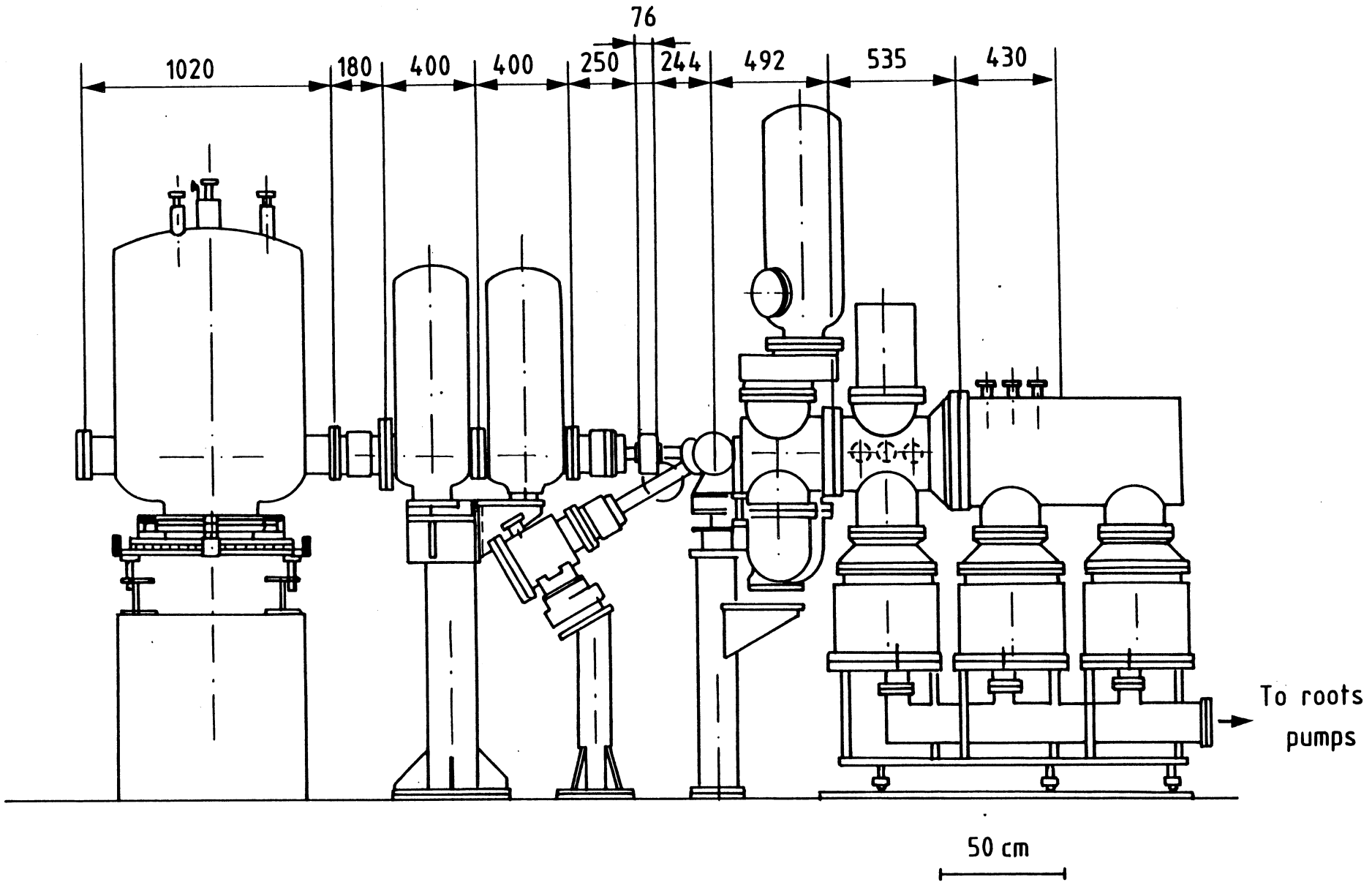

Fig. 1b

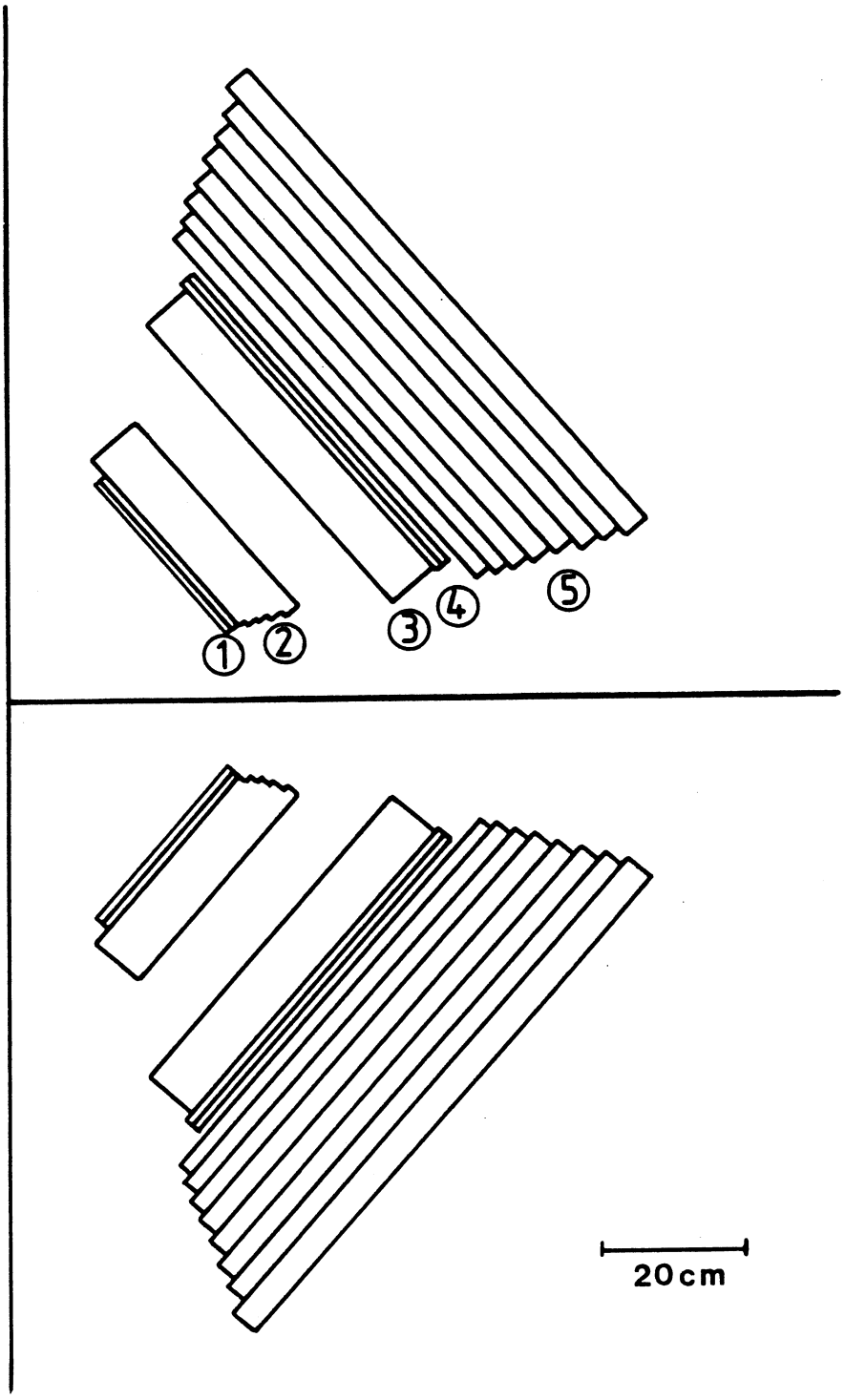

① ④ Scintillation counter hodoscopes
② ③ MWPC
⑤ Range detector

Fig. 2a

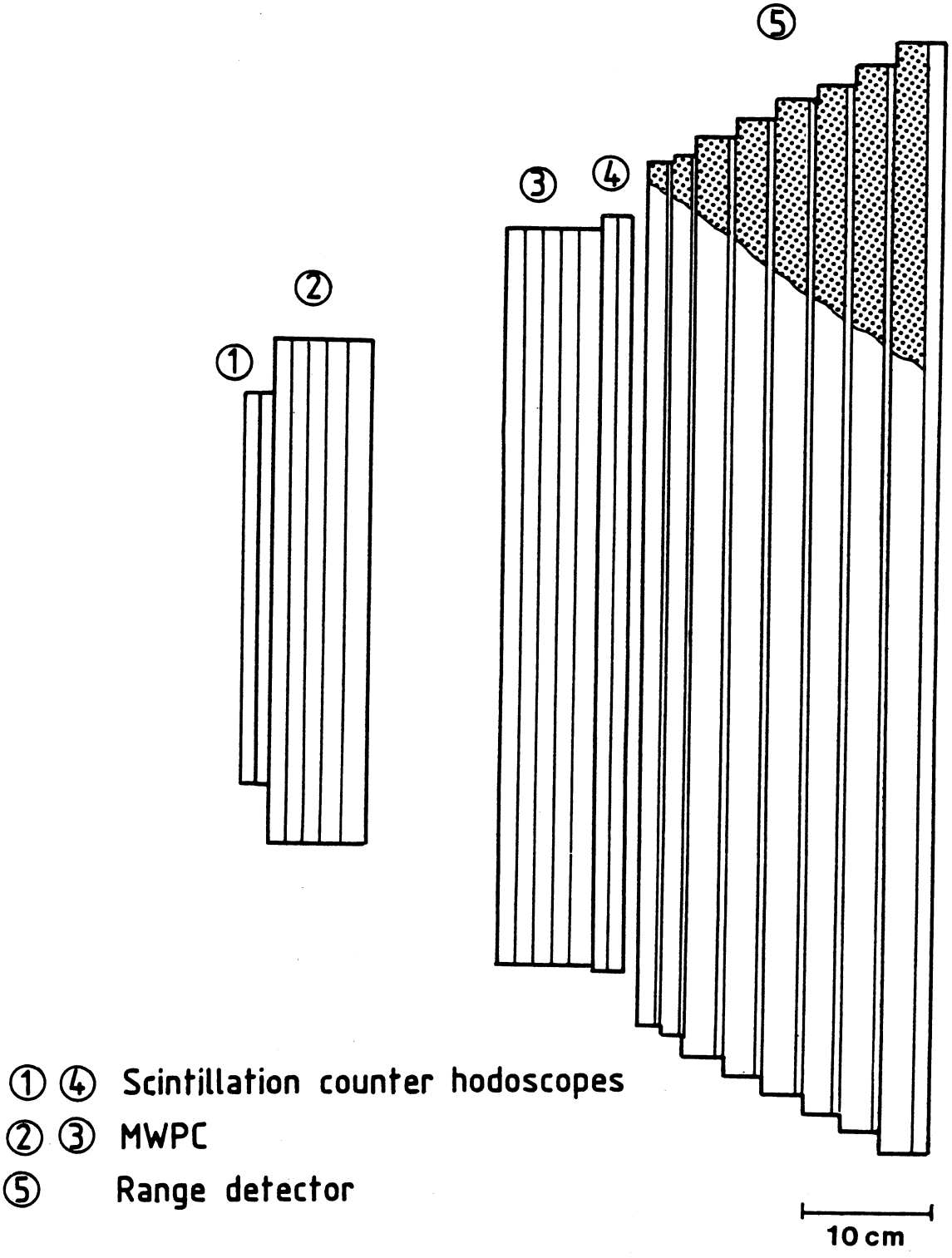
⑤
③
④
②
①
① ④ Scintillation counter hodoscopes
② ③ MWPC
⑤ Range detector
10 cm

Fig. 2b

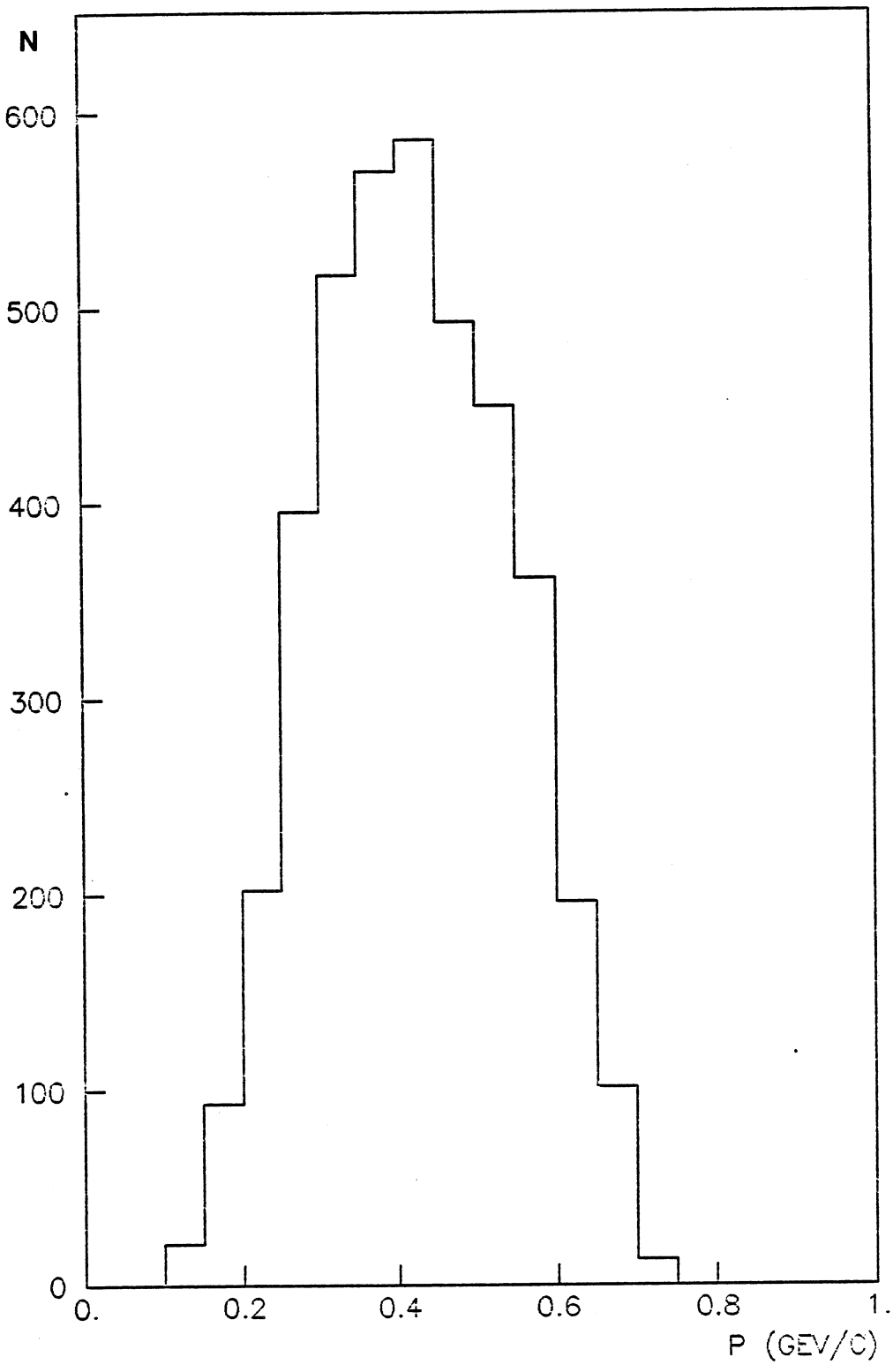

Fig. 3

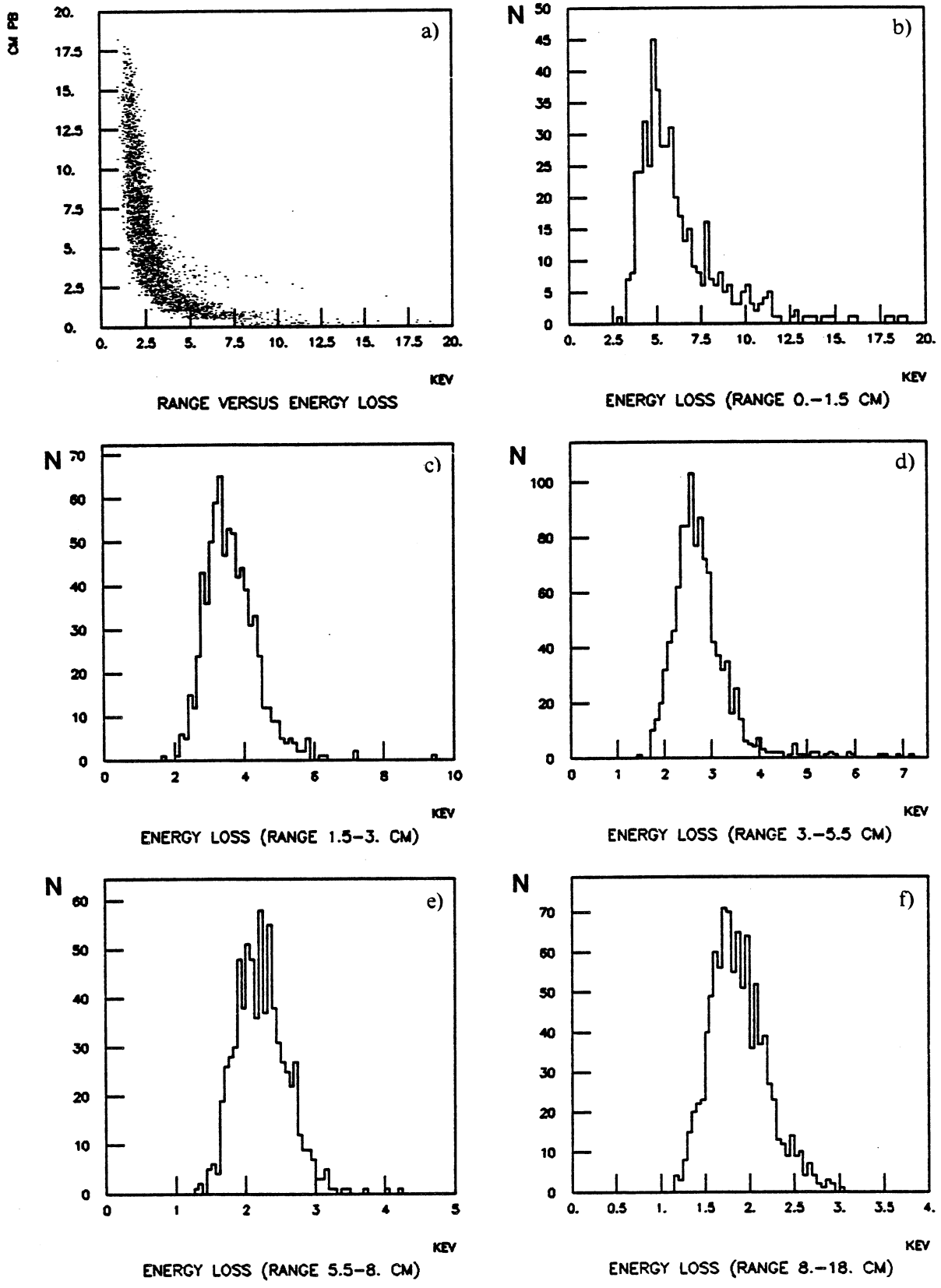
CM PB
a)
KEV
RANGE VERSUS ENERGY LOSS
N
b)
KEV
ENERGY LOSS (RANGE 0.–1.5 CM)
c)
KEV
ENERGY LOSS (RANGE 1.5–3. CM)
d)
KEV
ENERGY LOSS (RANGE 3.–5.5 CM)
e)
KEV
ENERGY LOSS (RANGE 5.5–8. CM)
f)
KEV
ENERGY LOSS (RANGE 8.–18. CM)

Fig. 4

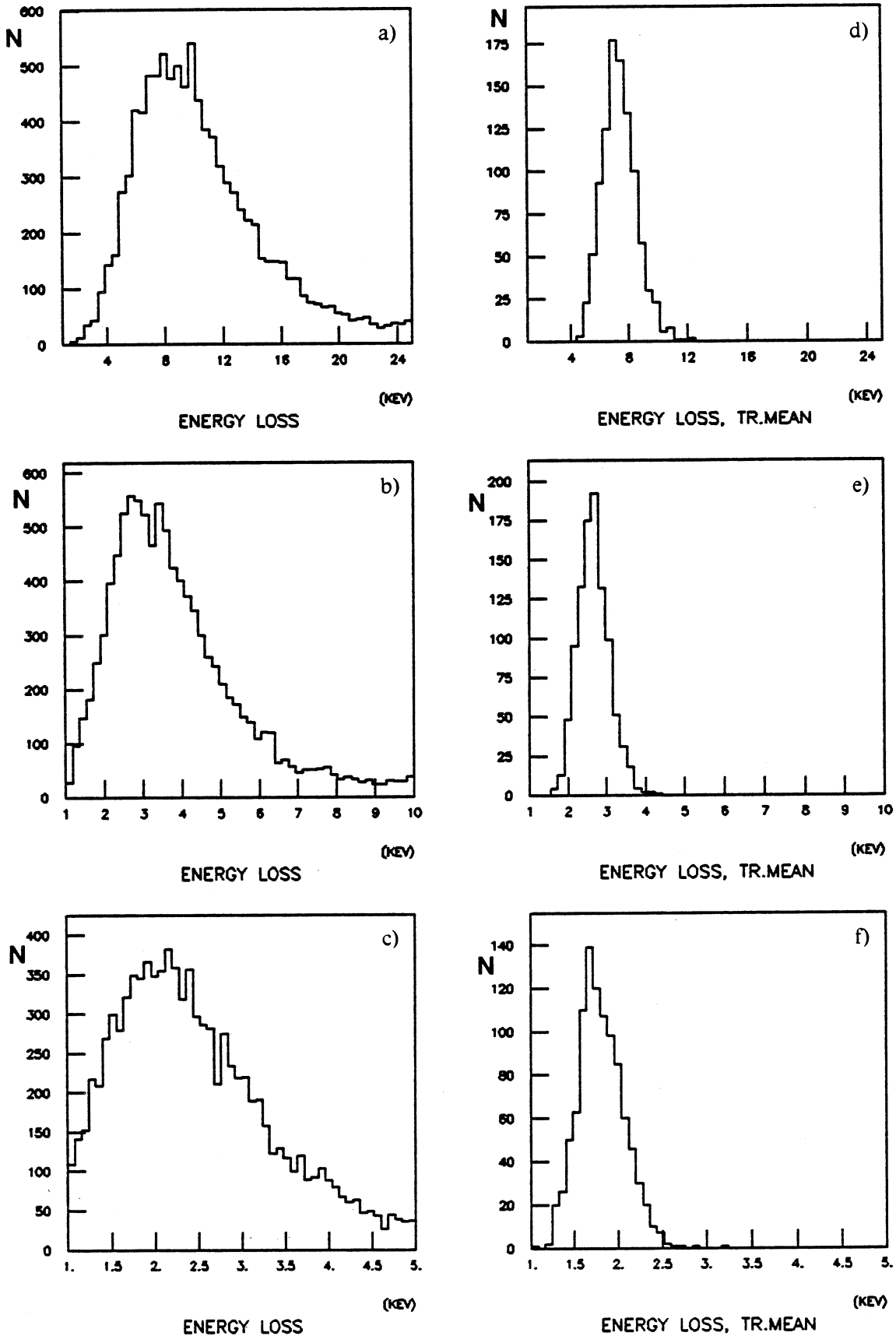
a)
N
ENERGY LOSS
(KEV)
d)
N
ENERGY LOSS, TR.MEAN
(KEV)
b)
N
ENERGY LOSS
(KEV)
e)
N
ENERGY LOSS, TR.MEAN
(KEV)
c)
N
ENERGY LOSS
(KEV)
f)
N
ENERGY LOSS, TR.MEAN
(KEV)

Fig. 5

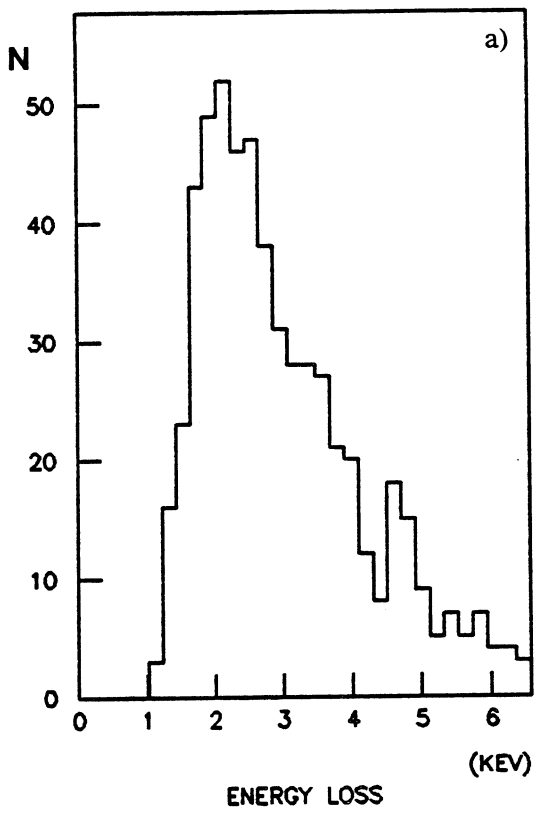
a)
N
50
40
30
20
10
0
0
1
2
3
4
5
6
(KEV)
ENERGY LOSS

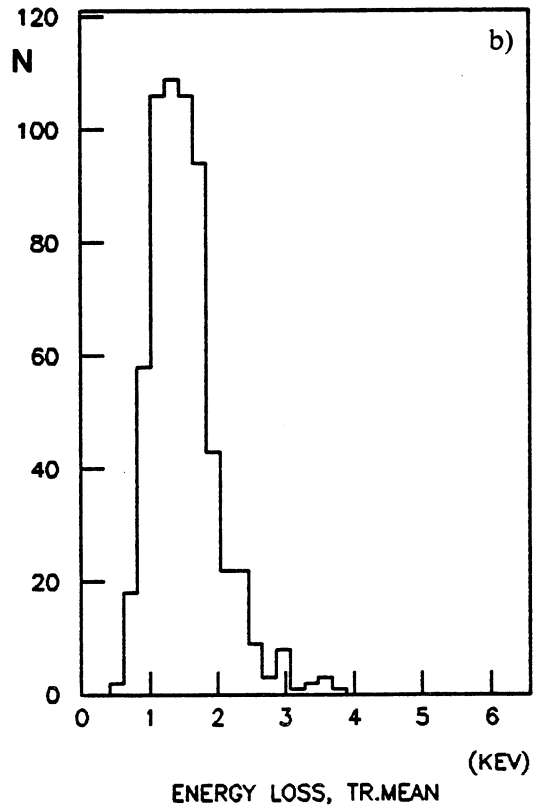
b)
N
120
100
80
60
40
20
0
0
1
2
3
4
5
6
(KEV)
ENERGY LOSS, TR.MEAN

Fig. 6

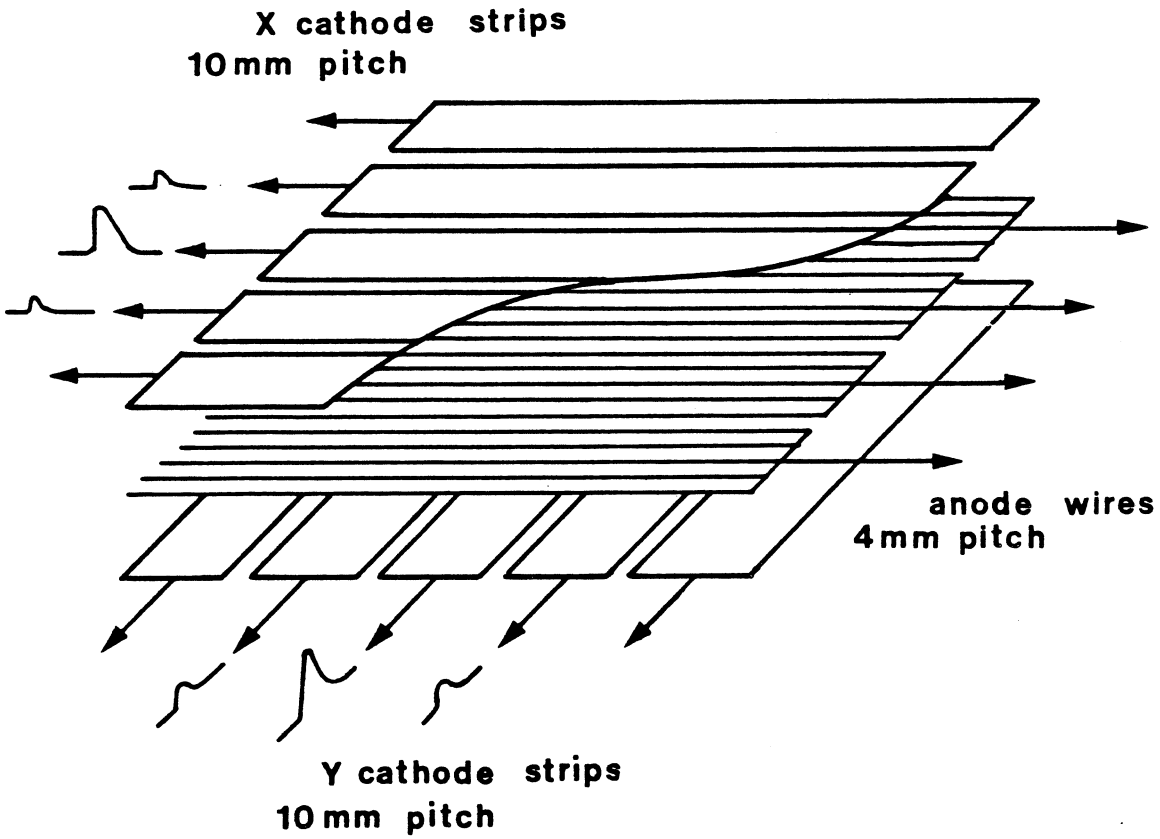
X cathode strips
10 mm pitch
anode wires
4 mm pitch
Y cathode strips
10 mm pitch

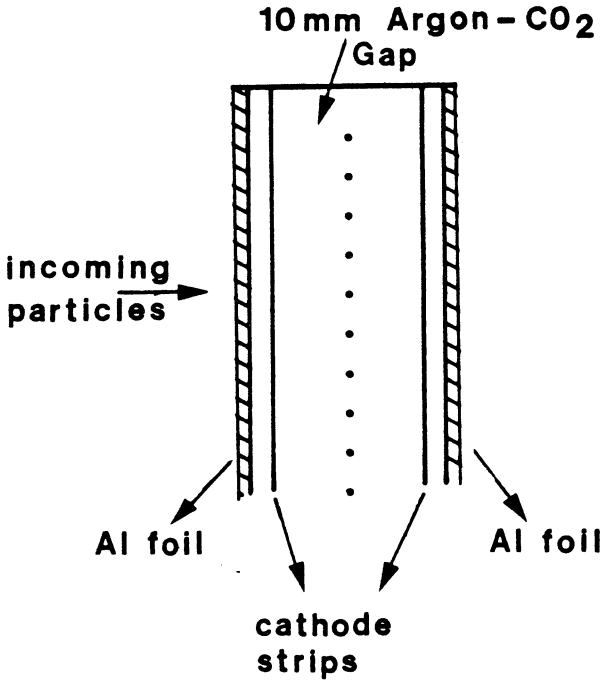
10 mm Argon – CO_2
Gap
incoming
particles
Al foil
Al foil
cathode
strips

Fig. 7

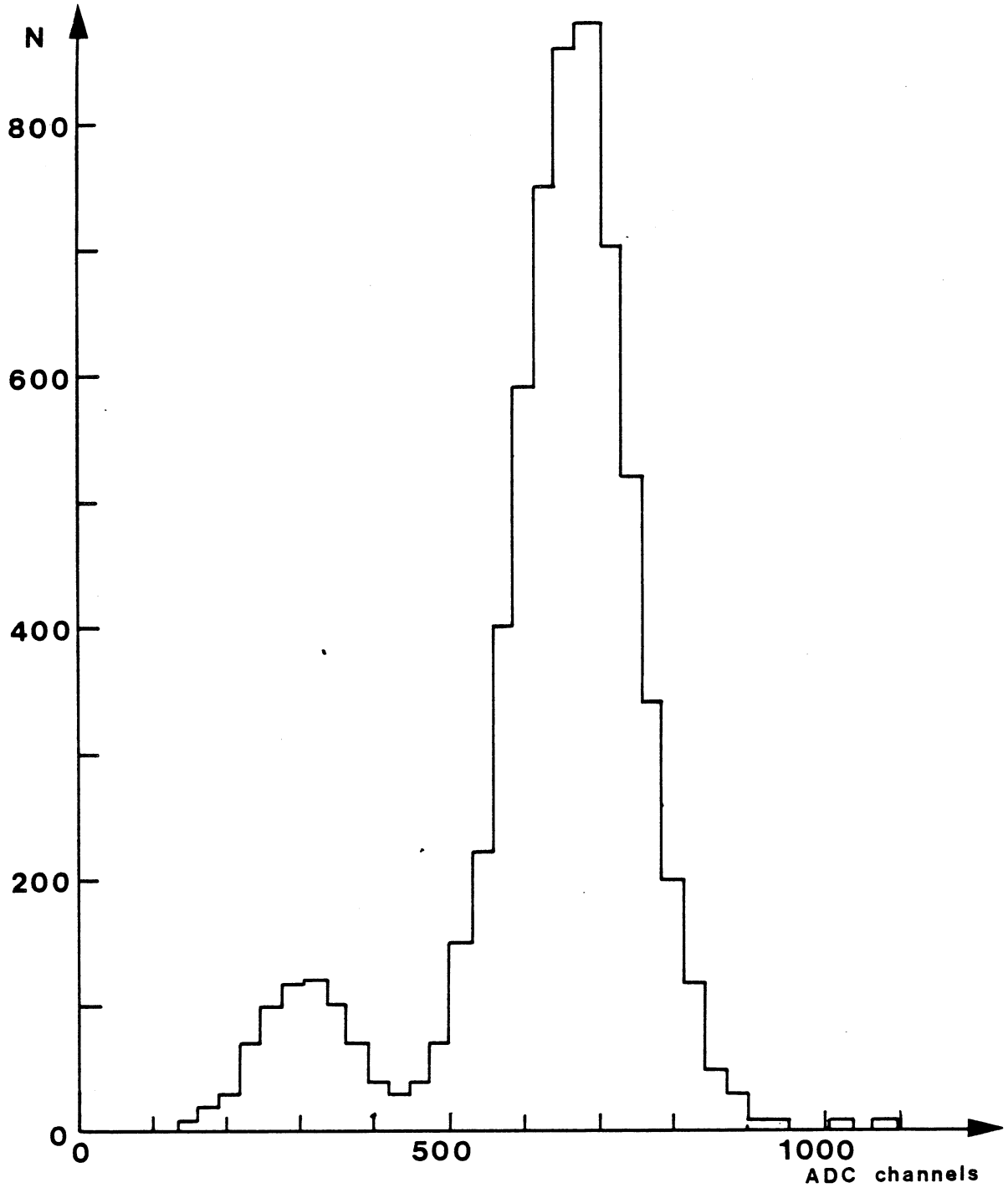

Fig. 8

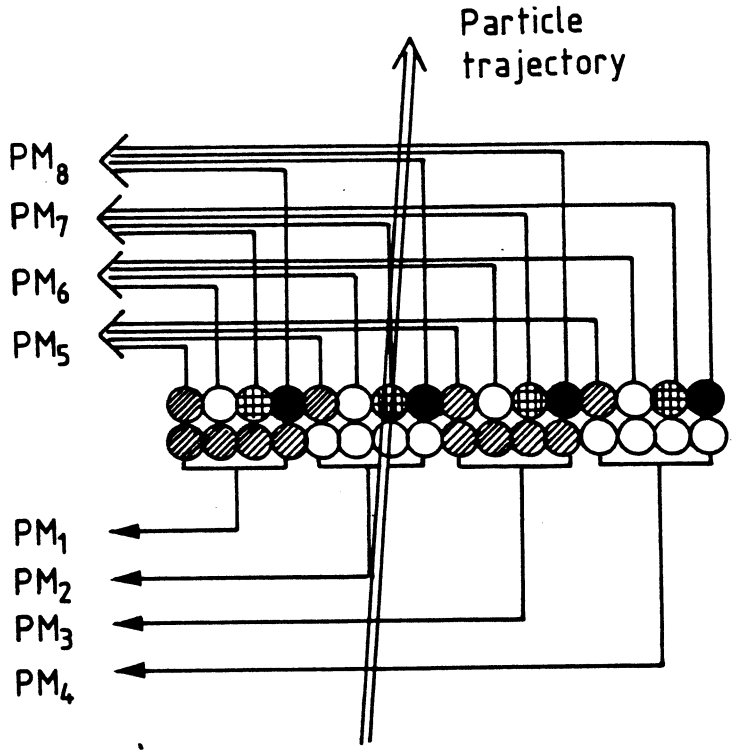

Fig. 9